

98
99
100
101
102
103
104
105
106
107
108
109
110
111
112
113
114
115
116
117
118
119
120
121
122
123
124
125
126
127
128
129

Figure S1. Cell distribution and abundance in the integrated COVID-19 PBMC data. (A)

Distributions of COVID-19 conditions (Left) and data sources (Right) for the integrated PBMC data are shown on the same UMAP of Figure 2A. (B) Bar plot depicts distributions of disease conditions in 5 individual PBMC single-cell datasets. Percentages of 3 disease conditions in each dataset is shown on y axis. (C) The integrated bar plot shows percentages of 3 disease conditions in each cell type per dataset. Dataset abbreviations and cell types were concatenated to show disease distributions of specific cell types in the selected datasets. These labels are colored by their cell type designations and ordered by the ascending percentages of COVID-19 conditions.

Figure S2. Dynamic changes of cell type abundances in five COVID-19 PBMC datasets.

Relative abundances and differences of major cell types in each single cell dataset are shown and compared to controls per each disease condition, per each single-cell dataset. Box plots of all cell types in PBMC are shown except for the 5 highlighted cell types shown in Figure 2B. Statistical methods are the same with Figure 2B.

Figure S3. Cell distributions and dynamic changes in the integrated COVID-19 BAL data.

(A-C) Distributions of disease conditions (A), data sources (B) and samples (C) are shown on the same UMAP of Figure 2C. (D) Box plots depict dynamic changes of cell types across COVID-19 conditions in BAL that are not covered in Figure 2D. Statistical methods are the same with Figure 2B.

Figure S4. Cell type abundance changes in COVID-19 lung parenchyma dataset. Box plots

depict percentages of cell types in control samples and severe COVID-19 samples. We used cell type clusters identified in the original publication but modified cell naming of macrophage

30 subtypes to distinguish monocyte derived macrophage subtypes present in BAL fluid samples.
31 Statistical methods are the same with Figure 2B.

32

33 **Figure S5. Sub-cluster-specific genes of neutrophils of COVID-19 patients.** (A) Distribution
34 of disease conditions (Left) and data sources (Right) for the integrated neutrophil data on the
35 same UMAP of Figure 3A. (B) UMAPs of neutrophil sub-cluster-associated genes from Figure
36 3C. Normalized expression values for each gene were used. (C) Normalized expression values of
37 neutrophil-associated genes and other important immune signatures are shown for 5 neutrophil
38 sub-clusters. Lowly expressed genes (genes with maximal average expression level across all
39 neutrophil sub-clusters less than 0.5 after Log₂CPM normalization) were removed from the gene
40 pool of cytokines, chemokines, ISGs, interleukins, interferons, corresponding receptors and
41 MHC-II. (D) The volcano plot depicts differentially expressed genes between circulating mature
42 neutrophils (Neu0,1) and extravasated neutrophils (Neu3) (Left); as well as DEGs between pro-
43 neutrophils (Neu4) and pre-neutrophils (Neu2) (Right). Statistical methods are the same with
44 Figure 5C. Representative enriched biological processes (Gene Ontology) are shown in the
45 bottom.

46

47 **Figure S6. Macrophage-related signatures in the integrated BAL data.** (A) Normalized
48 expression values of myeloid-cell-associated genes and other important immune signatures are
49 shown for 9 macrophage sub-clusters. Lowly expressed genes (genes with maximal average
50 expression level across all macrophage sub-clusters less than 0.5 after Log₂CPM normalization)
51 were removed from the gene pool of MHC-II, cytokines, chemokines, ISGs, interleukins,
52 interferons and their receptors. (B) Volcano plots were drawn for DEGs of MoAM3,4 versus
53 MoAM1,2,5 (Left) and TRAM 1,2 versus TRAM3 (Middle) and TRAM3 versus MoAM1,2,5
54 (Right). Statistical methods are the same with Figure 5C. (C) Normalized expression values were
55 shown on the same UMAP of Figure 3B for important genes including macrophage signatures,
56 ISGs, interferons, receptors and MHC-II.

57

58 **Figure S7. A uniquely-activated monocyte-derived cell type (MoAM5) exhibits a broad**
59 **signature of cytokines, chemokines, and interleukins including IL6.** (A) Normalized
30 expression values of IL6 on the same reference UMAP of integrated BAL data as Figure 3B. (B)
31 Scale expression levels of IL6 for each macrophage sub-cluster on the violin plot. (C) Heatmap of
32 expression levels of pan-MoAM signatures and MoAM5-specific signatures in all myeloid cells in

53 both PBMC and BAL. **(D)** Network of functional and phenotypic associated pan-MoAM
54 signatures and MoAM5-specific signatures from (C). Associations were retrieved from ToppGene
55 enrichment results. IL6 is highlighted in the network. As a caveat, the MoAM5 subtype
56 represented a small fraction among the BAL MoAM subtypes and the majority of these cells were
57 observed in a single severely-affected individual.

58

59 **Figure S8. Cell type and cell subtype-specific divisions of cytokine, chemokine, and**
60 **interleukin signaling pathways in BAL of severe COVID-19 patients.** **(A)** Heatmap of
61 expression patterns of ligands and receptors in cytokine, chemokine, interleukin, CSF and TNFSF
62 signaling pathways across cell types of BAL in severe patients. Average normalized expression
63 values were shown and lowly expressed ligands or receptors (maximal normalized expression
64 value for a row in the heatmap < 0.5) were removed. To reduce bias, MoAM5 was removed
65 because cells in the cluster were mainly from one patient. Cell types that have less than 5% cells
66 from severe patients were removed, including TRAM1 and TRAM2. Neutrophils are highlighted
67 in the heatmap. **(B)** Interaction network of BAL cells in severe patients using CellChat. CCL,
68 CXCL and IL1 signaling pathways were shown. The width of edges represents the strength of
69 interactions and the size of nodes represents the abundance of cell types.

30

31 **Figure S9. Characteristics of sub-clusters of classical monocytes in the integrated COVID-**
32 **19 PBMC data.** **(A)** UMAPs of 4 sub-clusters (Left) and COVID-19 conditions (Right) of
33 classical monocytes are shown. Grey dots are other myeloid cells in the UMAP of integrated
34 PBMC myeloid data. **(B)** UMAPs of normalized expression values of specific signatures for
35 classical monocyte sub-clusters. **(C)** Normalized expression values of monocyte-associated genes
36 and other important immune signatures are shown for 4 classical monocyte sub-clusters. **(D)** Gene
37 modules of classical monocyte sub-clusters, as well as other myeloid cell types in the integrated
38 PBMC myeloid data. Representative genes in each module are shown on the left. ToppGene
39 enrichment results for classical monocyte sub-clusters are shown on the right. Columns are
40 clustered using hierarchical clustering. **(E)** Similarity matrix of myeloid cell types using genes in
41 (D). Pearson correlation was used to evaluate similarity. **(F)** Dot plot of MHC-II, ISGs,
42 interleukin genes and cell cycle genes for each myeloid cell type. Scale values were used.

33

34 **Figure S10. Features of conventional dendritic cell sub-clusters and polarized signaling**
35 **genes.** **(A)** UMAPs of 13 sub-clusters (Left) and sources (Right) of conventional dendritic cells

96 after data integration. **(B)** Normalized expression values of sub-cluster-specific genes on the
97 UMAP. **(C)** Normalized expression values of cDC-associated genes and other important immune
98 signatures are shown for 13 cDC sub-clusters. **(D)** Gene modules of cDC sub-clusters with 200
99 most significantly upregulated genes in each module. Representative genes are shown on the left.
100 Gene enrichment results of some modules from ToppGene are shown on the right. **(E)** Similarity
101 matrix of sub-clusters using genes in (D). Pearson correlation was used for similarity scores and
102 hierarchical clustering was applied for rows and columns. **(F)** The heatmap shows the clustering
103 of signaling genes, including cytokines, chemokines, interleukins and their receptors. Red boxes
104 highlight severe patients associated sub-clusters and their upregulated genes. Green boxes
105 highlight mild patients-associated sub-clusters and their upregulated genes.

106

107 **Figure S11. Landscape of myeloid cells in the integrated PBMC and BAL data. (A-B)**
108 UMAPs of myeloid cells in integrated PBMC (A) and BAL (B) data. Cell types which were
109 further clustered are highlighted in different colors. **(C)** The heatmap shows associations between
110 subclusters of myeloid cells and myeloid-cell-associated pathways, such as antigen presenting, T
111 cell activation, phagocytosis etc. Gene enrichment scores, defined as $-\log_{10}(\text{adjusted p value})$,
112 were calculated as the strength of associations. Pie charts showed the proportions of COVID-19
113 conditions in each sub-cluster.

114

115 **Figure S12. Gene expression signatures of cell types and subtypes activated by COVID-19**
116 **are extensively associated with coagulation, hemostasis, and thrombosis-associated**
117 **pathways, functions, and knockout phenotypes. (A)** Functional association heatmap of gene
118 signatures from COVID-19 cell types demonstrates differential enrichment for pathways
119 associated with coagulation, vascular permeability, complement, extravasation, platelet activation
120 and aggregation, response to wounding, as shown. Gene modules of cell types and sub-clusters
121 that participate in these pathways were used to calculate enrichment scores. **(B)** Network of
122 upregulated genes in coagulation/thrombosis-associated pathways (A) shows the potential gene-
123 gene interactions in immunothrombosis of COVID-19 patients. CellChat and ToppCell/ToppGene
124 protein-protein ligand receptor and cell adhesion interaction databases were used to find
125 interaction pairs among upregulated genes. **(C)** A new network derived from (B) shows integrin-
126 associated interactions between platelets and other cells.

127

28 **Figure S13. Emergence of platelet subtypes suggestive of functionally significant alternative**
29 **roles in in hemostasis, coagulation, wound response, and neutrophil recruitment and**
30 **activation. (A)** The heatmap shows ToppCell gene modules of 6 platelet sub-clusters in COVID-
31 19 PBMC. Each gene module contains 200 most significant genes for each sub-cluster and
32 important genes are shown on the left. Gene enrichment analysis was conducted using ToppGene
33 and top enrichment results from biological processes (Gene Ontology) are shown on the right. **(B)**
34 Dot plot of integrin and other platelet-associated genes. Scale values are shown on the figure. **(C)**
35 Heatmap of associations between subclusters of platelets and platelet-associated pathways (Gene
36 Ontology). Gene enrichment scores, defined as $-\log_{10}(\text{adjusted p value})$, were calculated and
37 shown.

38
39 **Figure S14. Consistent emergence of a series of early and maturing B cells and**
40 **plasmablasts in BAL fluid and PBMC across multiple datasets. (A-B)** UMAPs of B cells (A)
41 and plasmablasts (B) from multiple datasets. **(C-D)** UMAP of normalized expression values of
42 immunoglobulin genes (C) and ISGs (D) for B cells. **(E-F)** UMAP of normalized expression
43 values of immunoglobulin genes (E) and sub-cluster associated genes, such as cell cycle genes
44 and B cell markers (F) for plasmablasts. **(G)** Gene modules of B cell sub-clusters and plasmablast
45 subtypes with 200 most significant genes in each module. Hierarchical clustering was applied for
46 columns. **(H)** Three representative enriched biological processes (Gene Ontology) are shown for
47 these two subtypes using DEGs of plasmablasts in Figure 5C.

48
49 **Figure S15. Gene Enrichment analysis of B cell subtypes and autoimmune-associated**
50 **signatures. (A)** Heatmap shows gene enrichment scores of B-cell-associated pathways for each B
51 cell sub-cluster and plasmablast subtype. **(B)** Pathway and function association network of
52 upregulated genes in B cells of BAL in mild COVID-19 patients. **(C-D)** Heatmaps show
53 normalized expression levels of autoimmune-associated ligands and receptors (Figure 5E) in
54 lupus nephritis (C) and rheumatoid arthritis (D).

55
56 **Figure S16. Distinct subtypes of T cells and NK cells in COVID-19 BAL data. (A-C)** UMAPs
57 of subtypes (A), COVID-19 conditions (B) and data sources (C) of T cells and NK cells in the
58 integrated BAL data. **(D-E)** UMAPs of normalized expression values of exhausted T cell markers
59 **(D)** and ISGs **(E)**.

30

51 **Figure S17. Various T cell and NK cell subtypes in the integrated PBMC data. (A-B)**
52 UMAPs of T cell and NK cell subtypes (A) and COVID-19 conditions (B) after integration of T
53 cells in 5 PBMC single-cell datasets. (C) Dot plot shows T cell and NK cell subtype associated
54 genes for each subtype per disease condition. Labels of cell types of healthy donors, mild patients
55 and severe patients are colored by blue, yellow and red. Scaled expression values are shown using
56 a color scheme.

57
58 **Figure S18. Various cell types in immune-mediated diseases. (A, C, E) Distributions of cell**
59 **types identified in influenza (A), sepsis (C) and multiple sclerosis (E) patients were shown on**
60 **UMAPs. (B, D, F) Distributions of disease conditions in influenza (B), sepsis (D) and multiple**
61 **sclerosis (F) patients were shown on UMAPs.**

72

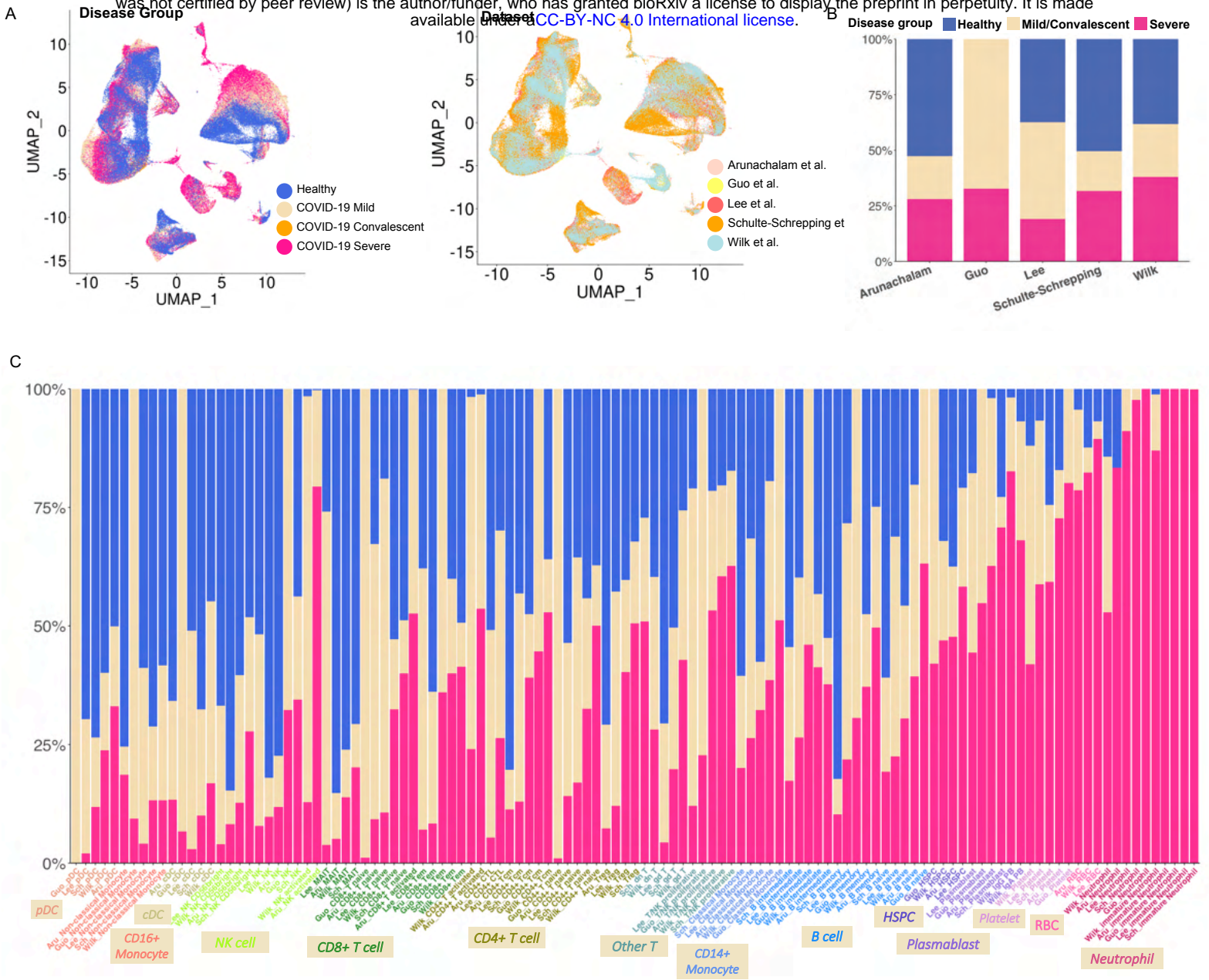


Figure S1. Cell distribution and abundance in the integrated COVID-19 PBMC data, relative to Figure 2.

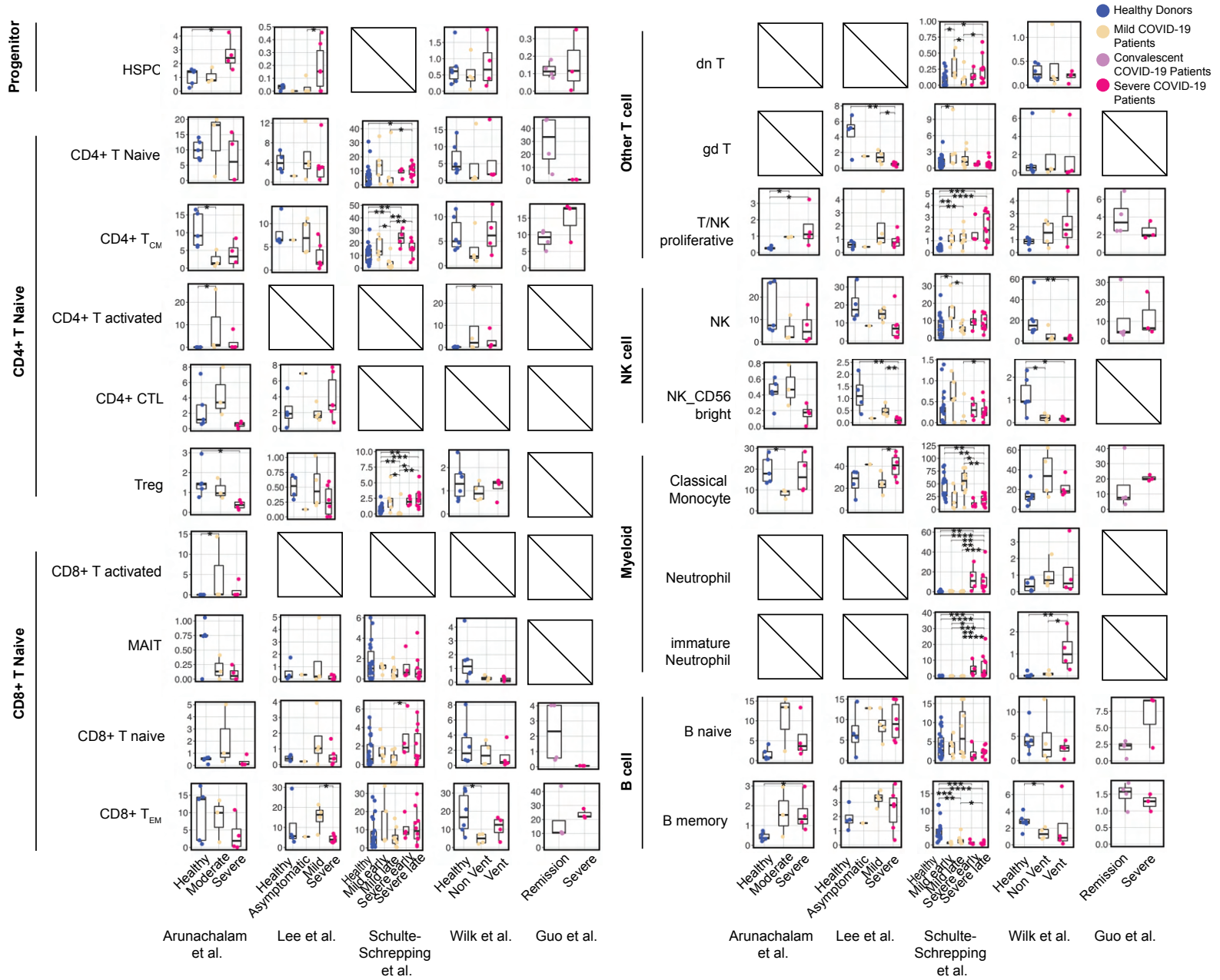


Figure S2. Dynamic changes of cell type abundance in the integrated PBMC data, relative to Figure 2.

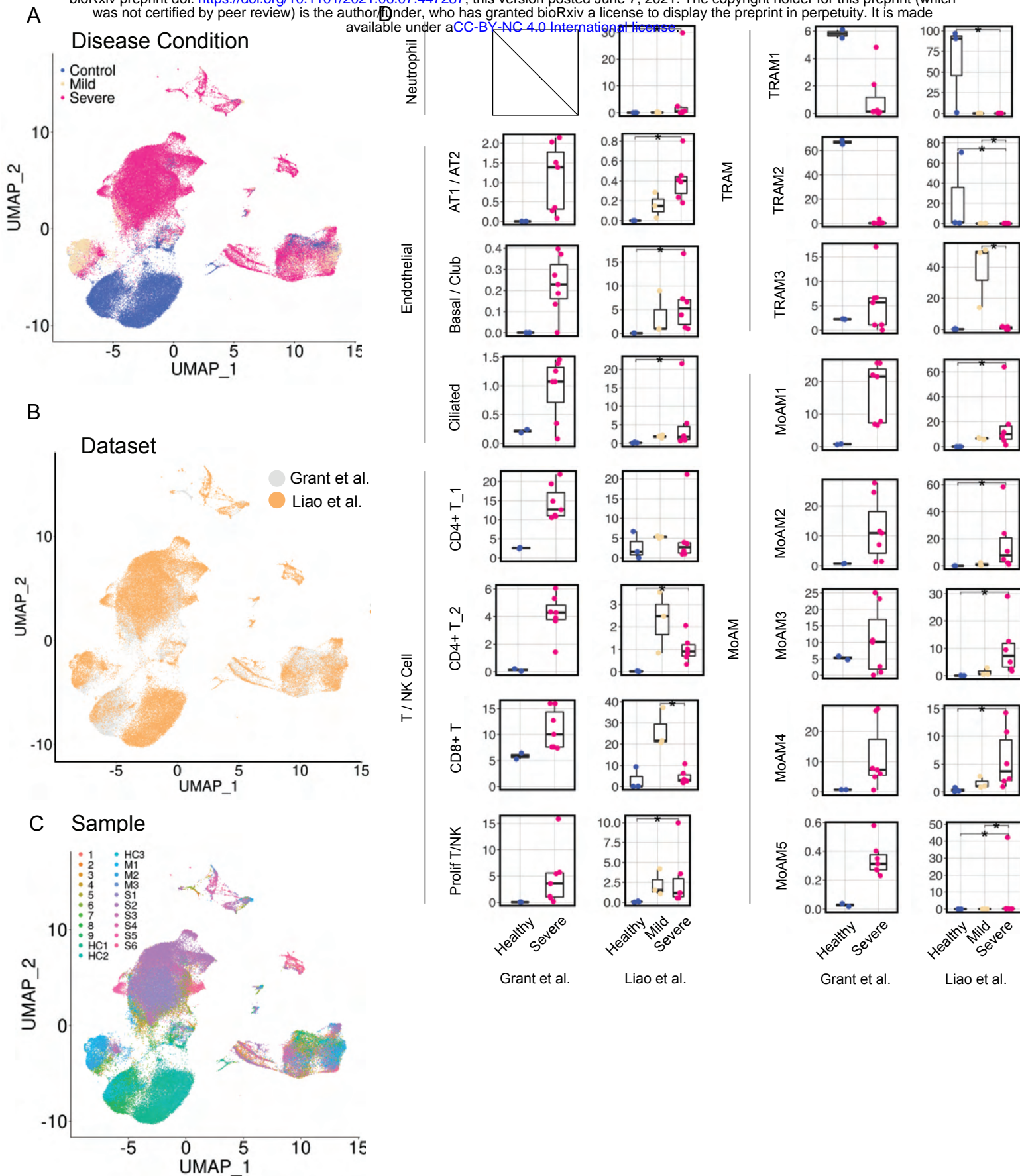


Figure S3. Cell distributions and dynamic changes in the integrated COVID-19 BAL data, relative to Figure 2.

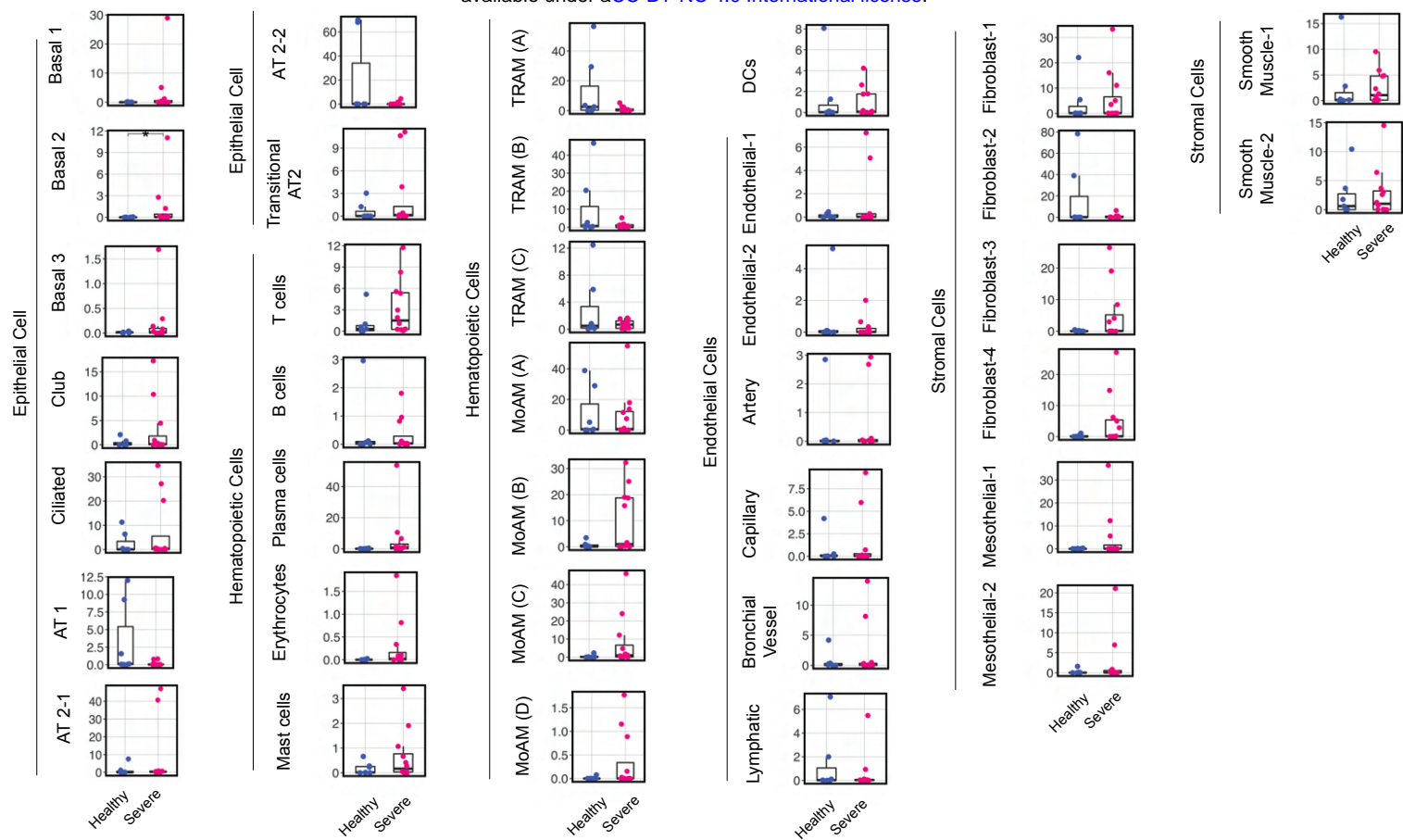
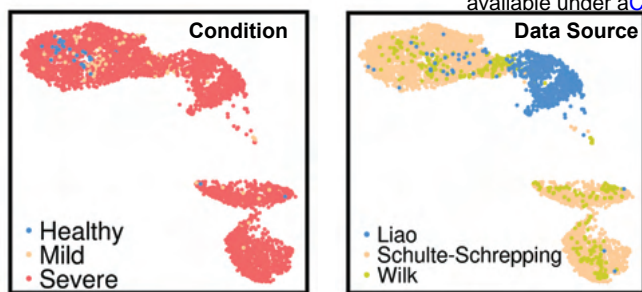
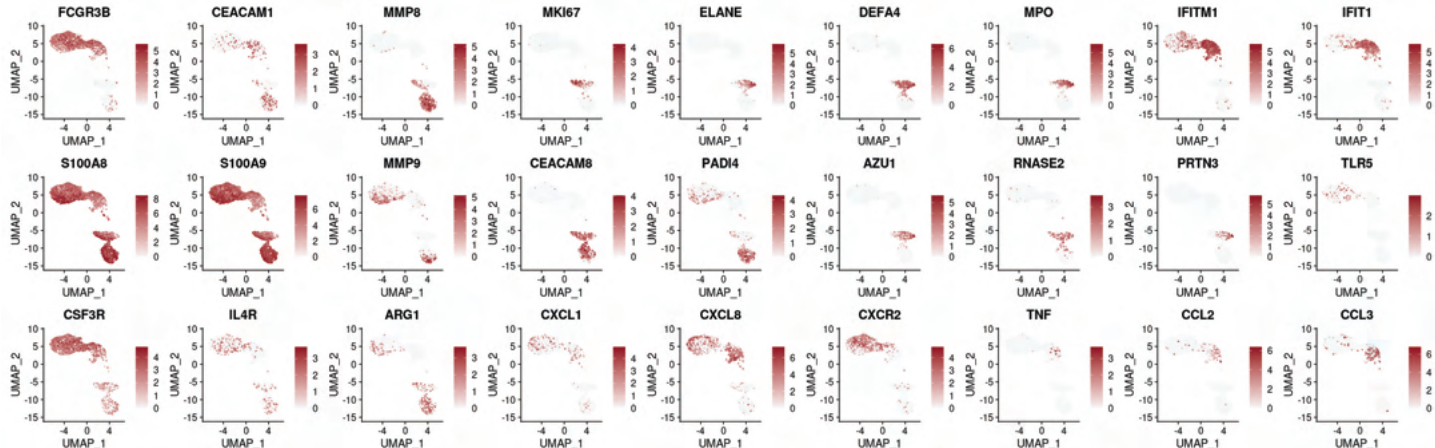


Figure S4. Dynamic changes of cell types in the COVID-19 lung parenchyma dataset, relative to Figure 2.

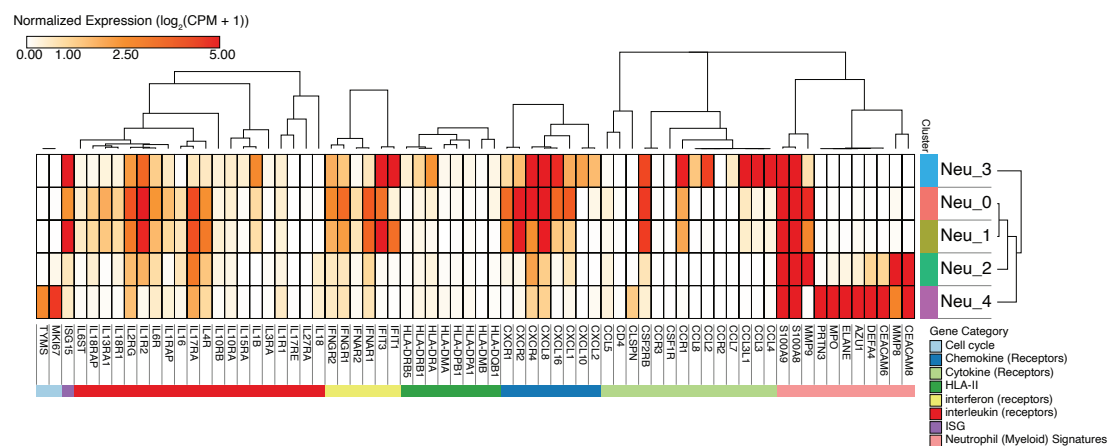
A



B



C



D

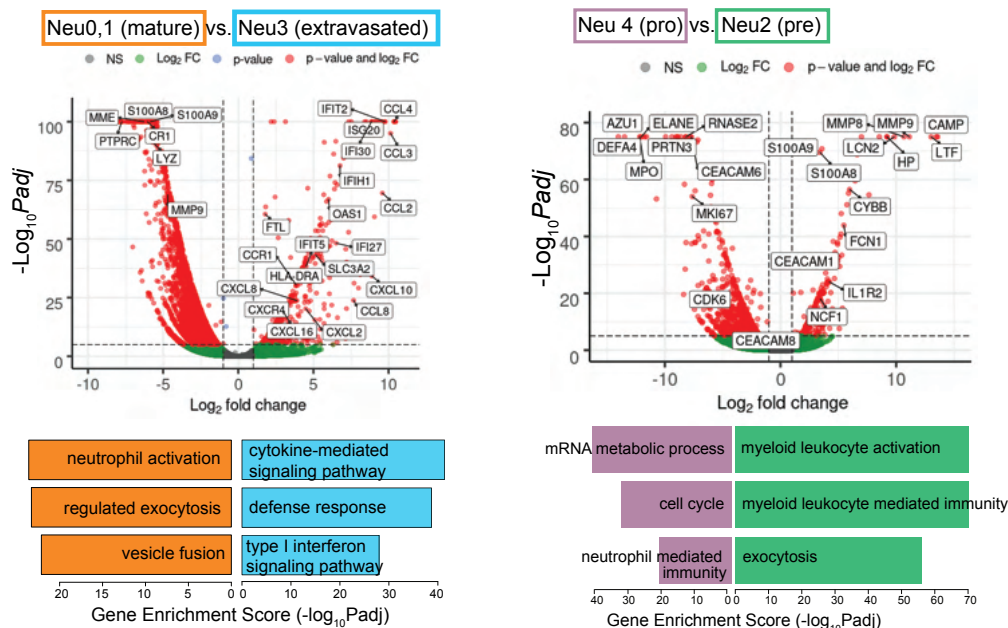
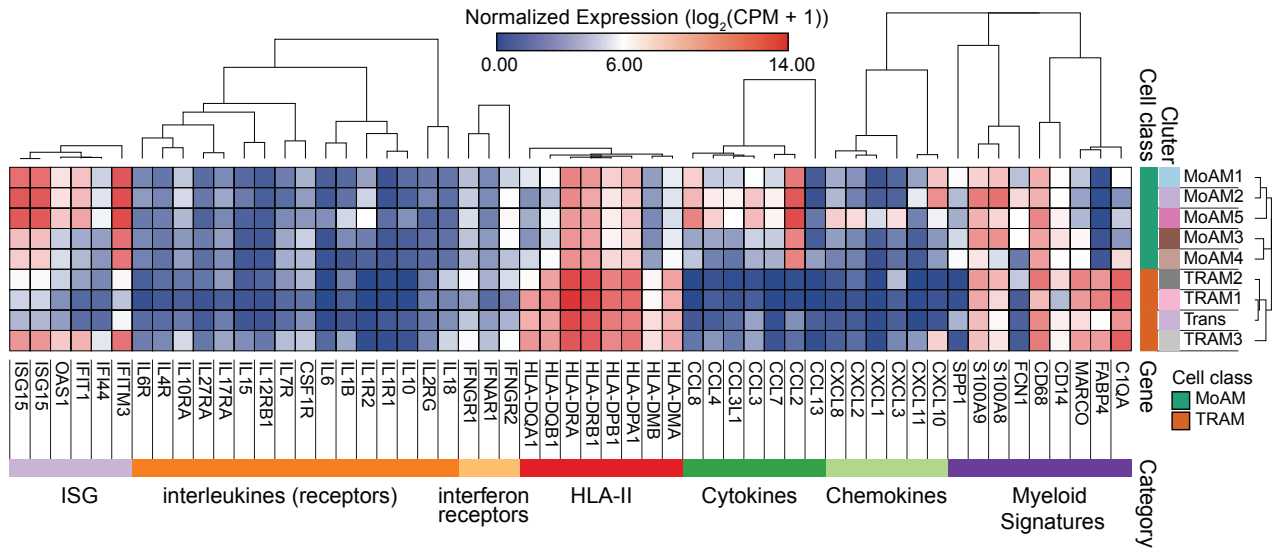
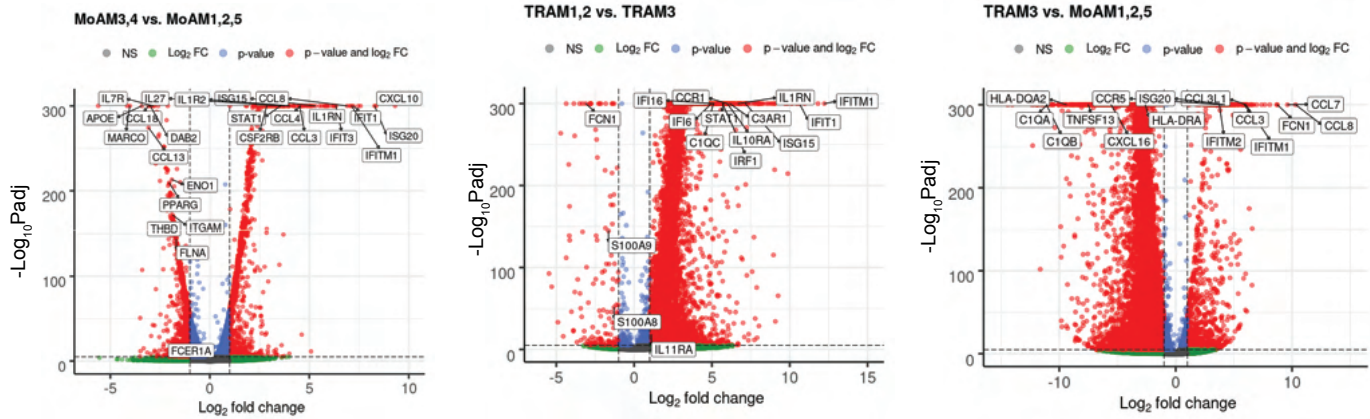


Figure S5. Sub-cluster-specific genes of neutrophils of COVID-19 patients, relative to Figure 3.

A



B



C

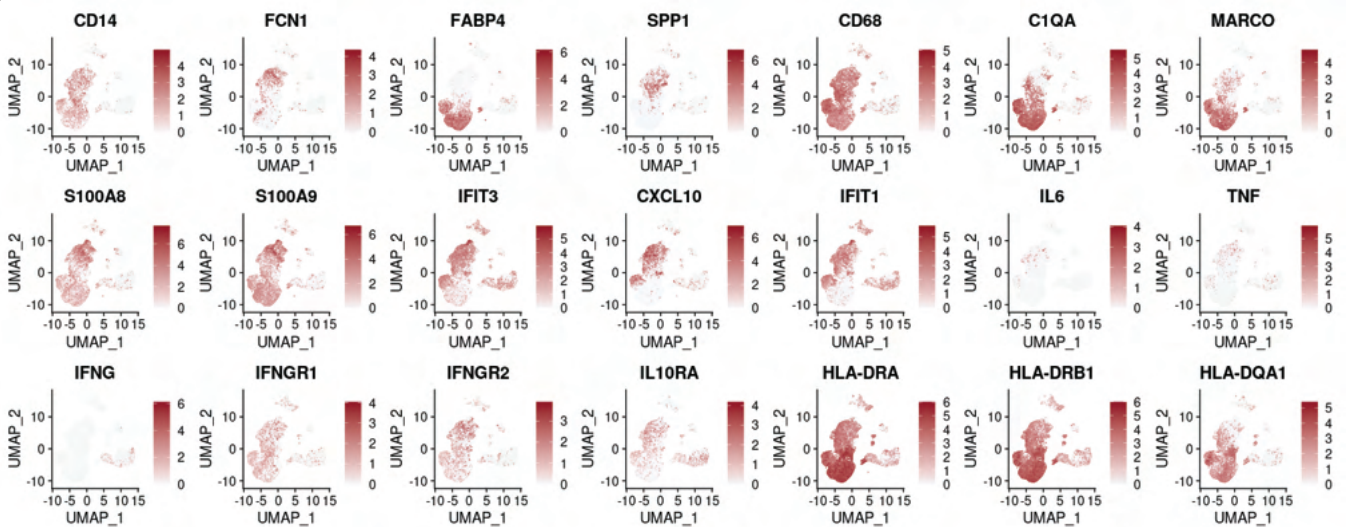


Figure S6. Macrophage-related signatures in the integrated BAL data, relative to Figure 3.

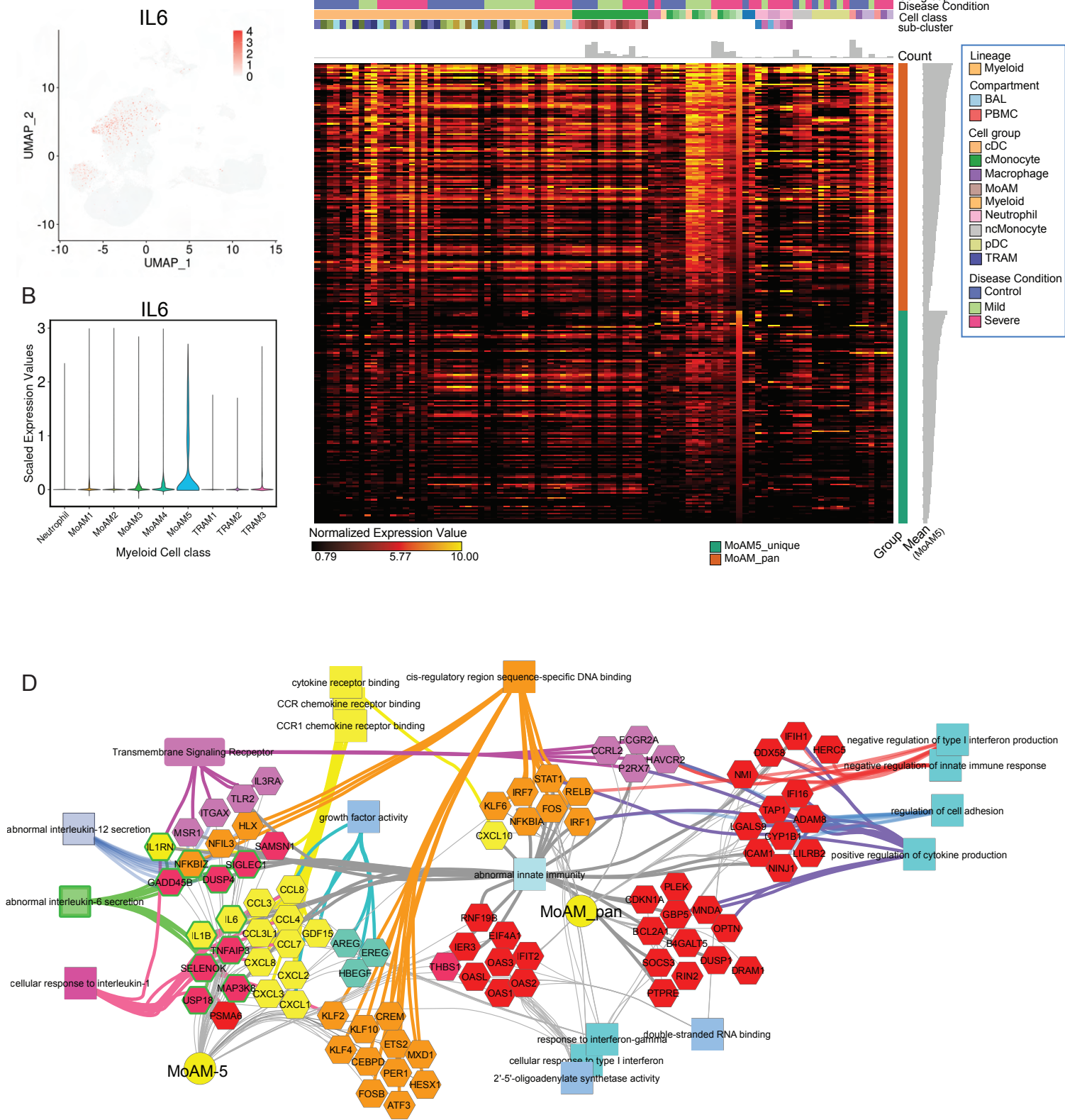


Figure S7. A uniquely-activated monocyte-derived cell type (MoAM5) exhibits a broad signature of cytokines, chemokines, and interleukins including IL6, relative to Figure 3.

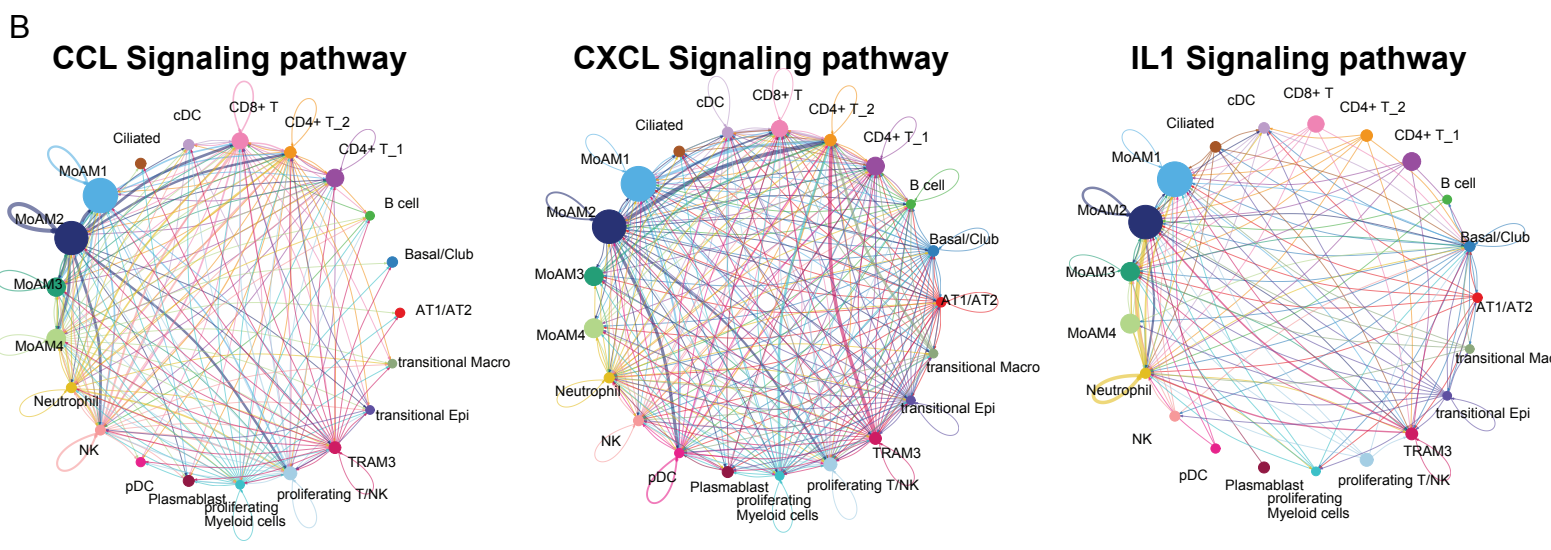
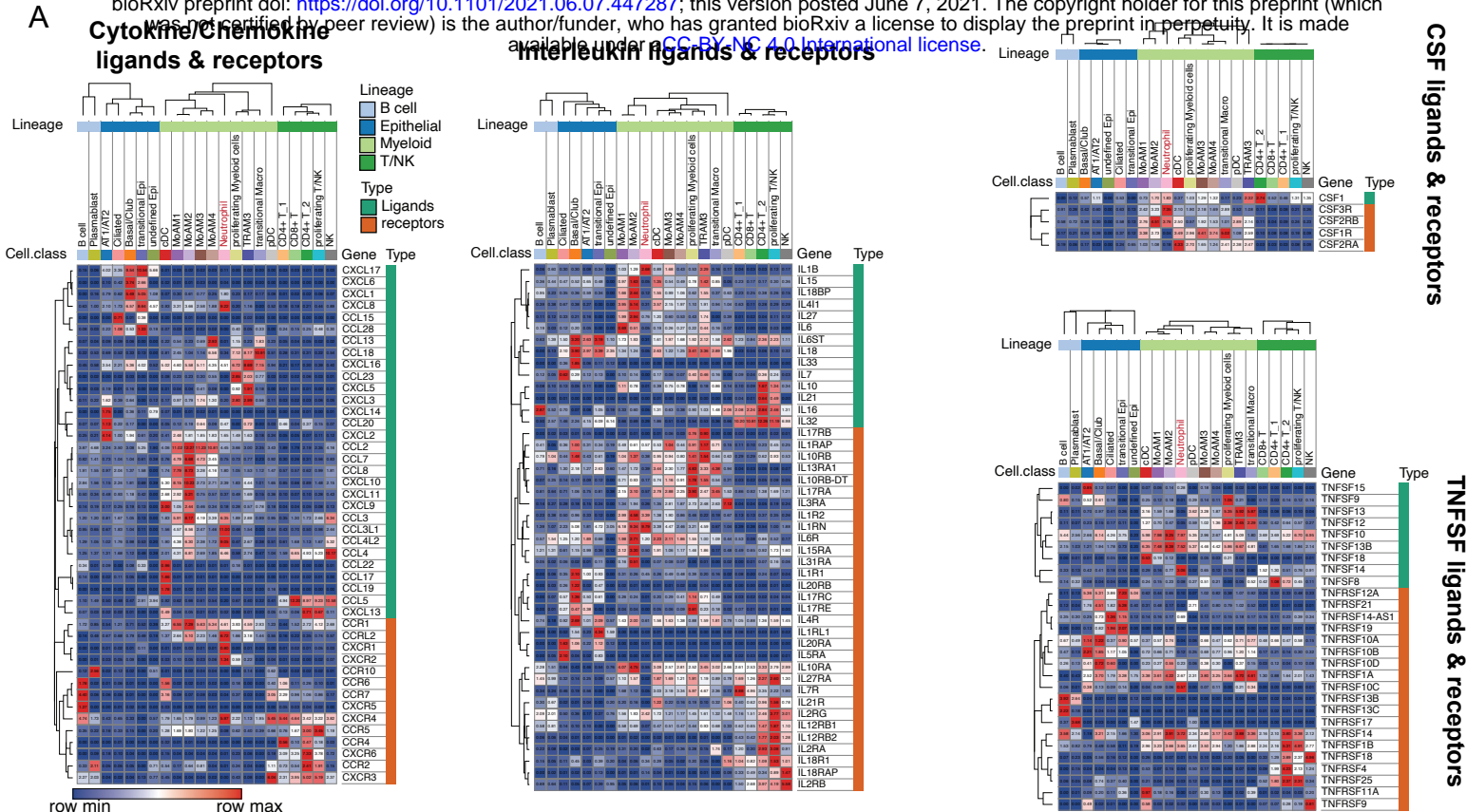
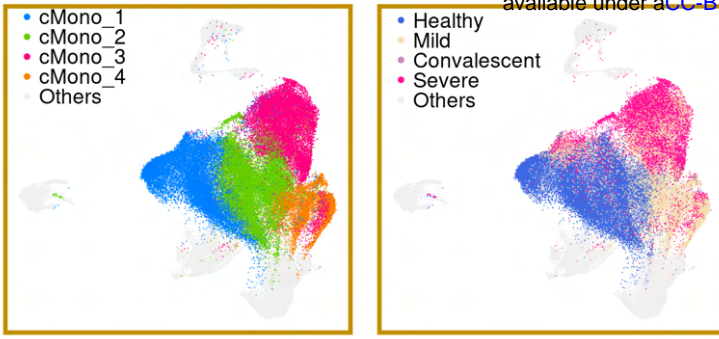
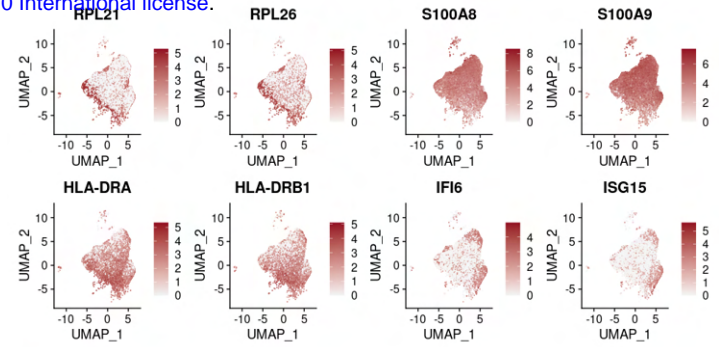


Figure S8. Cell type and cell subtype-specific divisions of cytokine, chemokine, and interleukin signaling pathways in BAL of severe COVID-19 patients, relative to Figure 3.

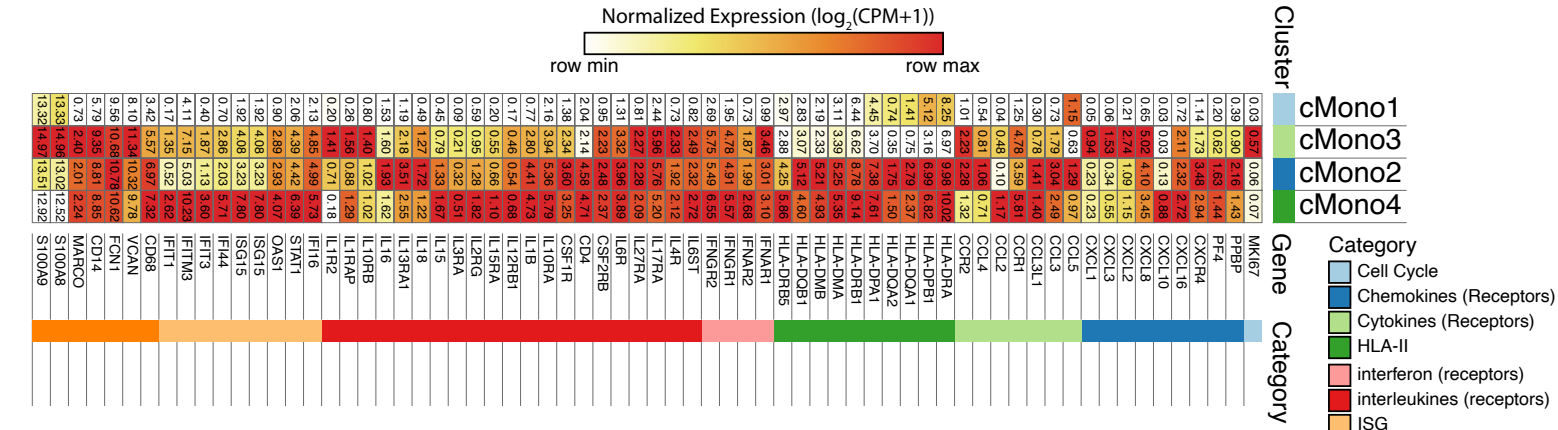
A



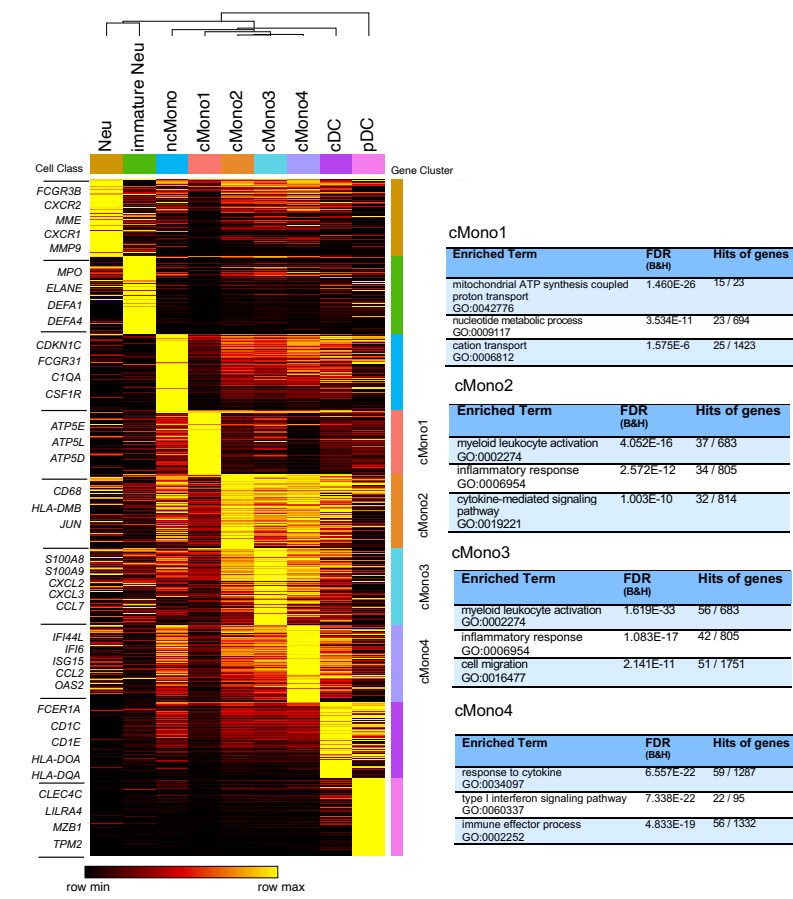
B



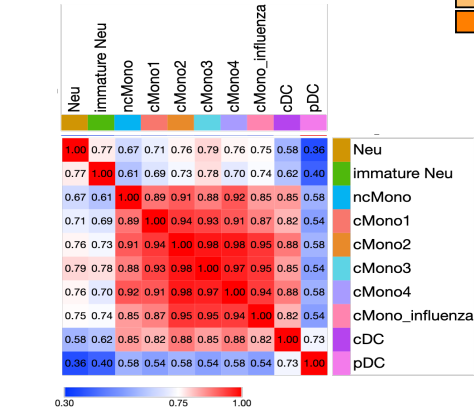
C



D



E



F

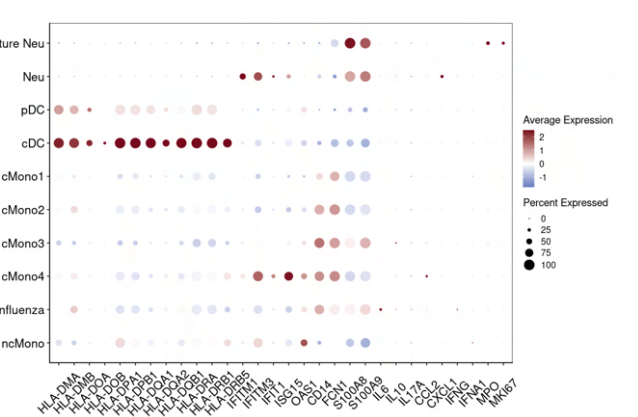
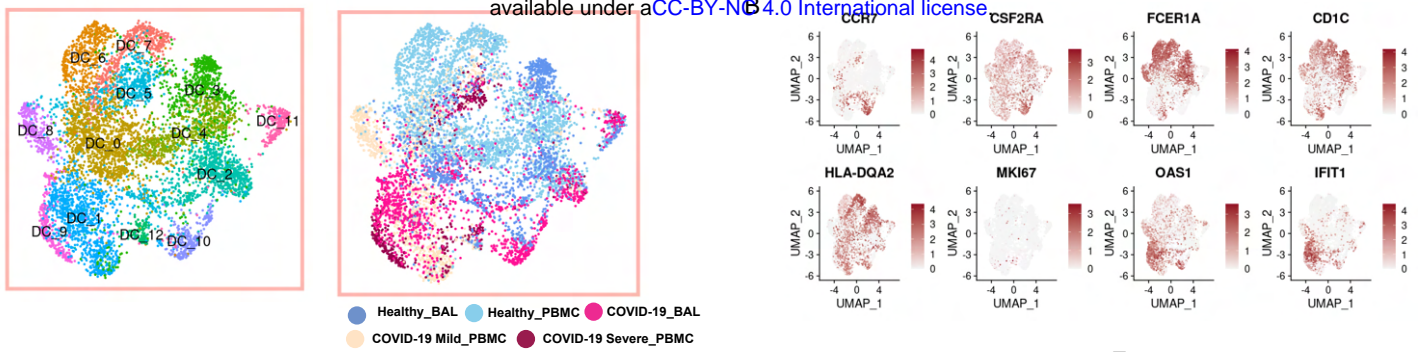
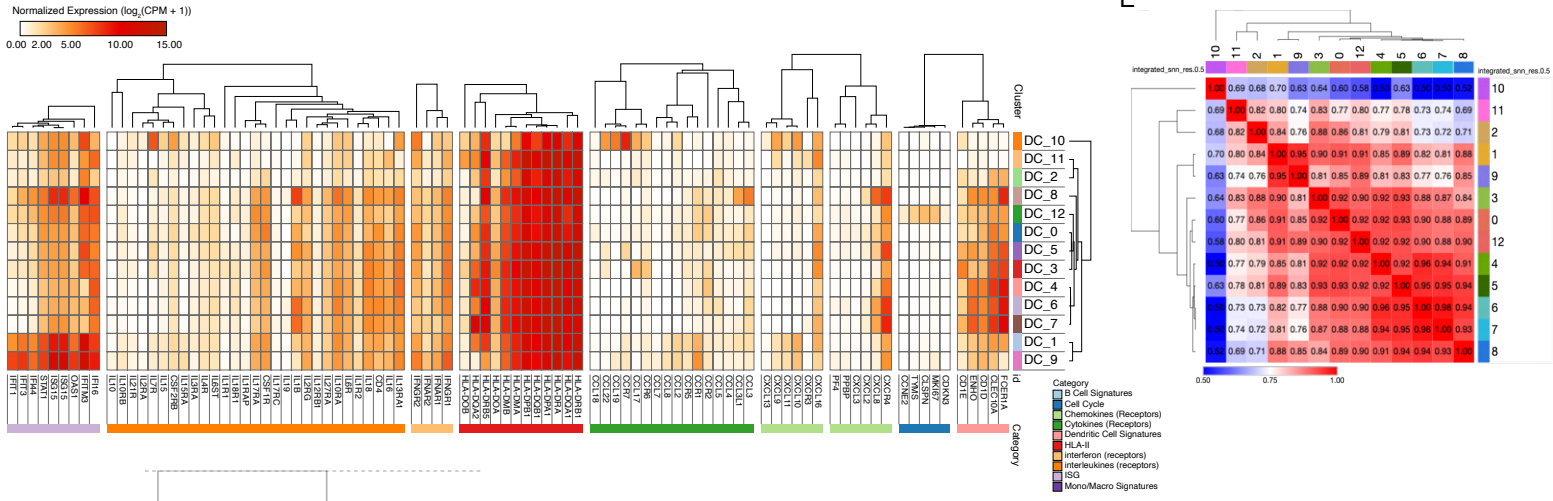


Figure S9. Characteristics of sub-clusters of classical monocytes in the integrated COVID-19 PBMC data, relative to Figure 3.

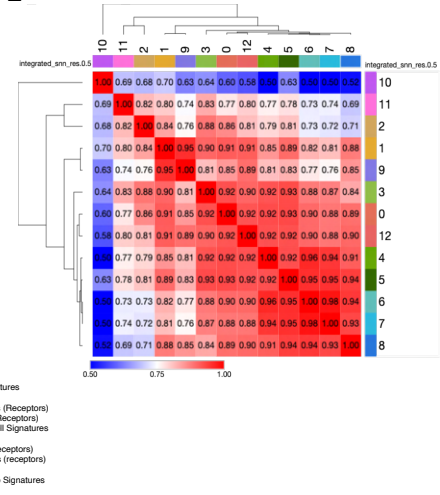
A



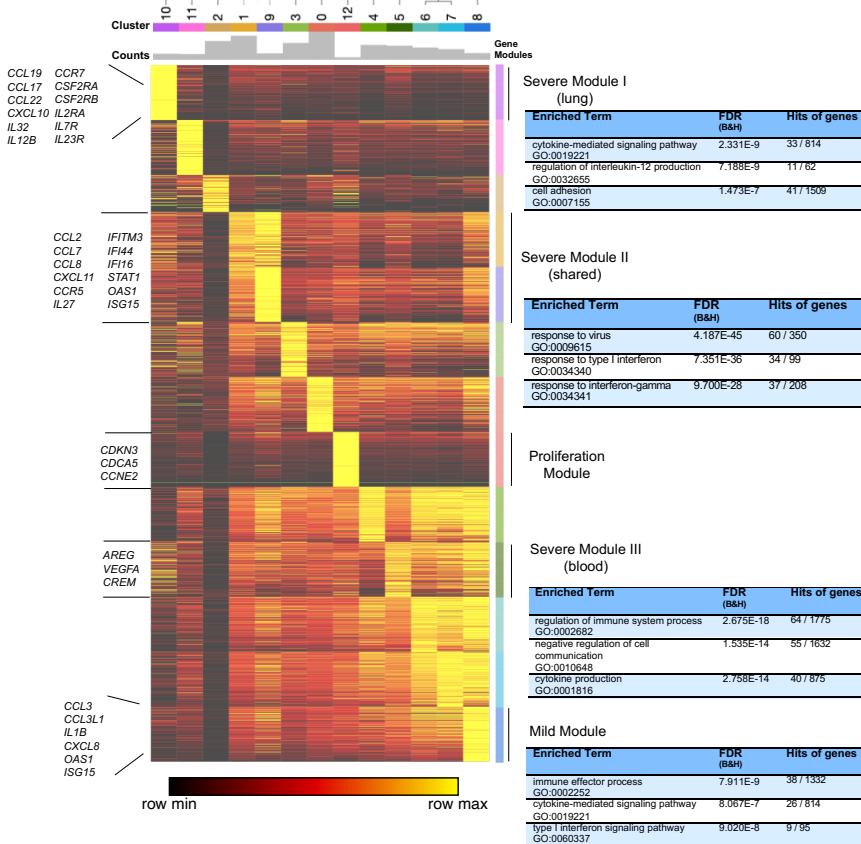
C



E



D



F

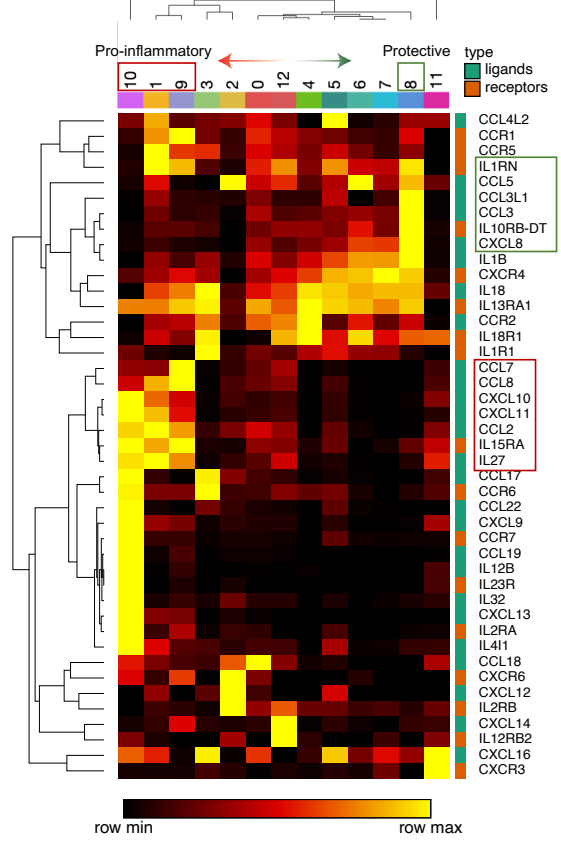
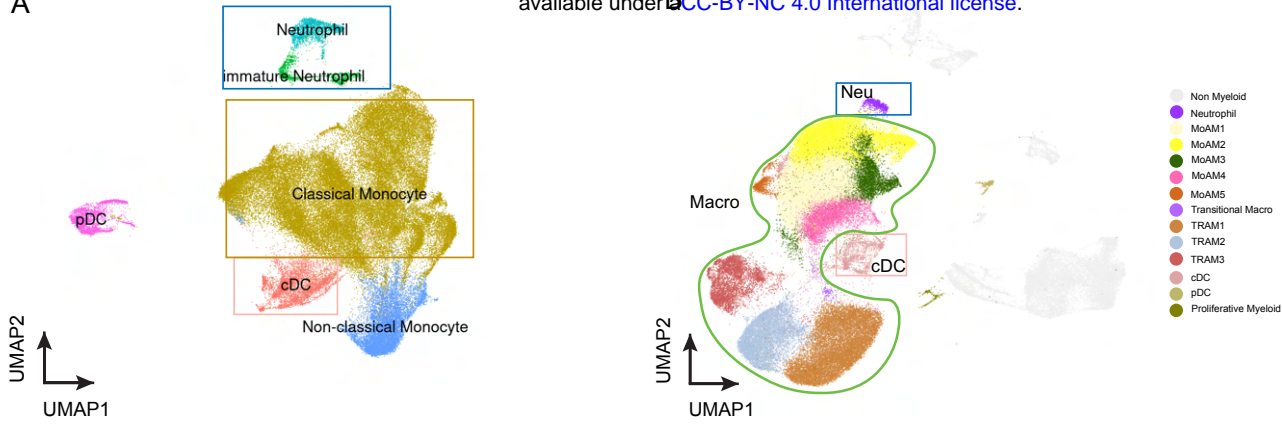


Figure S10. Features of conventional dendritic cell sub-clusters and polarized signaling genes, relative to Figure 3.

A



C



Figure S11. Landscape of myeloid cells in the integrated PBMC and BAL data, relative to Figure 3.

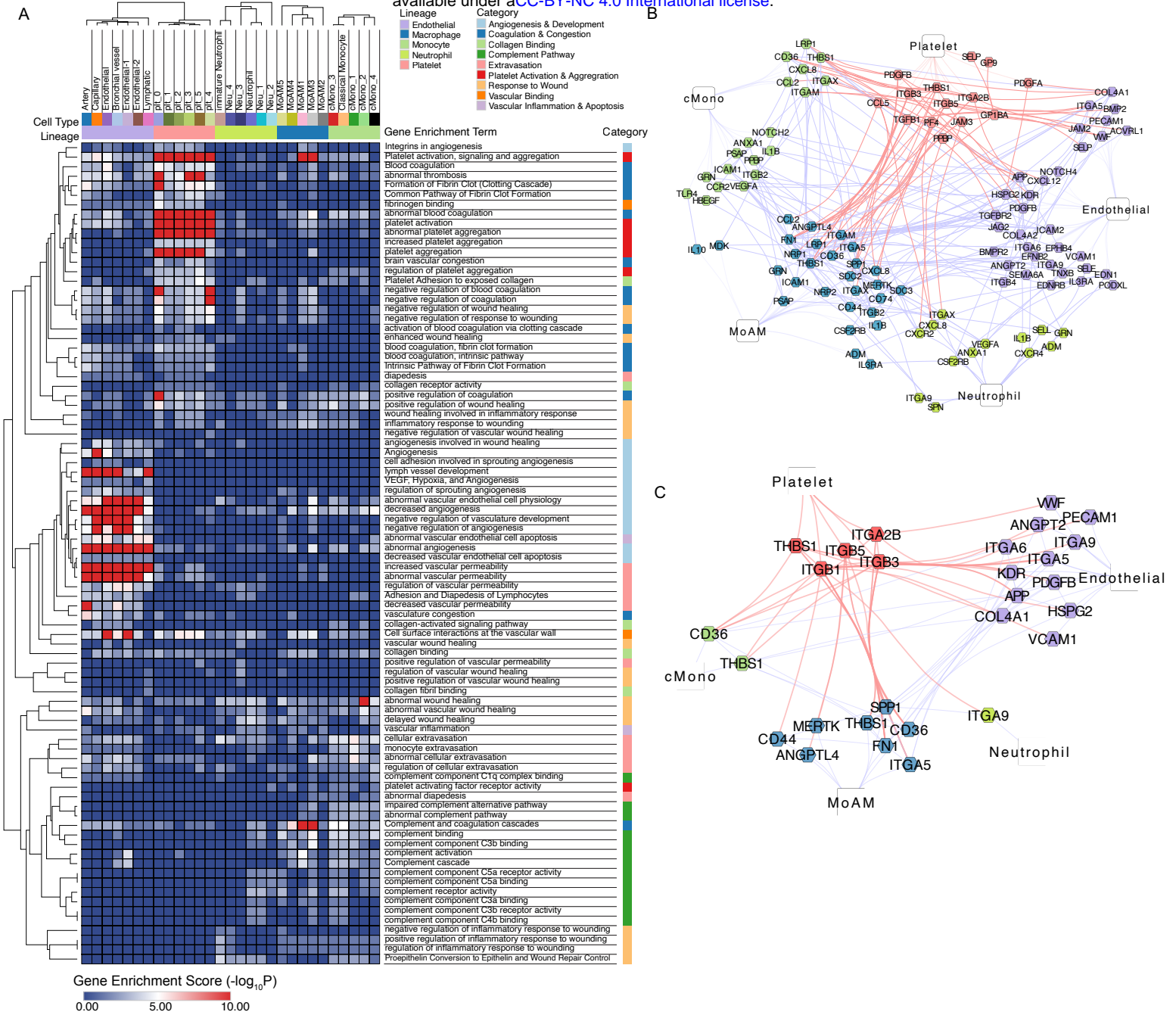
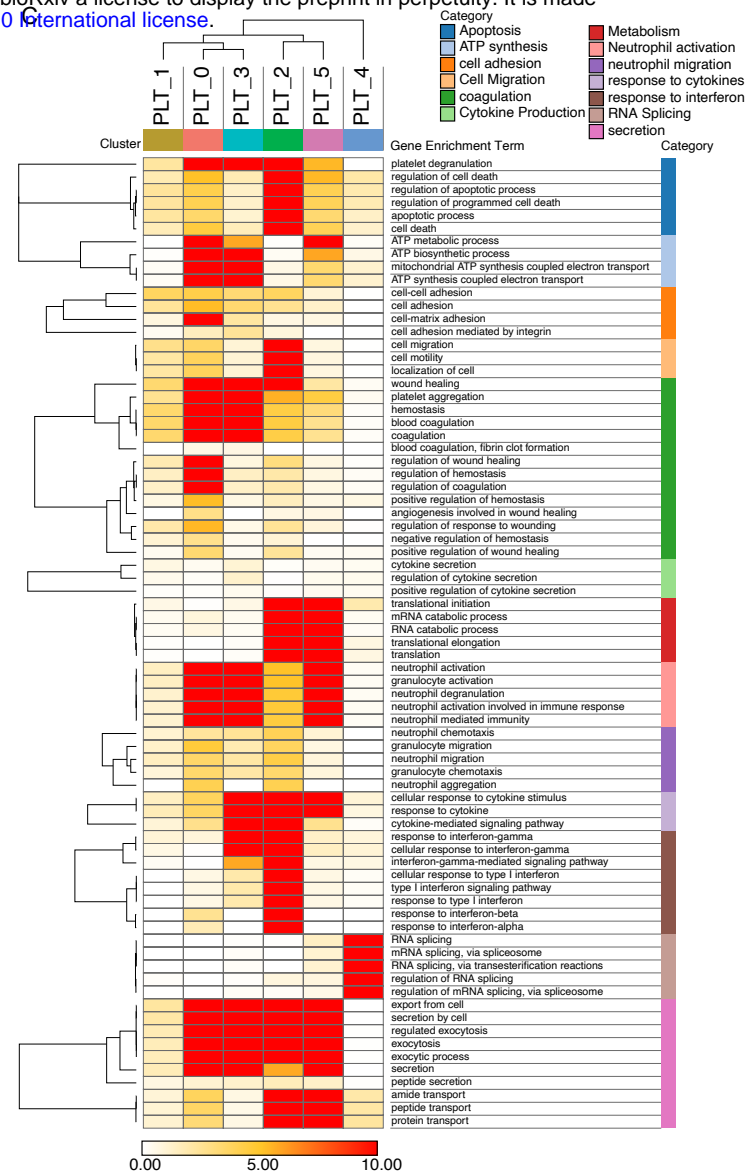
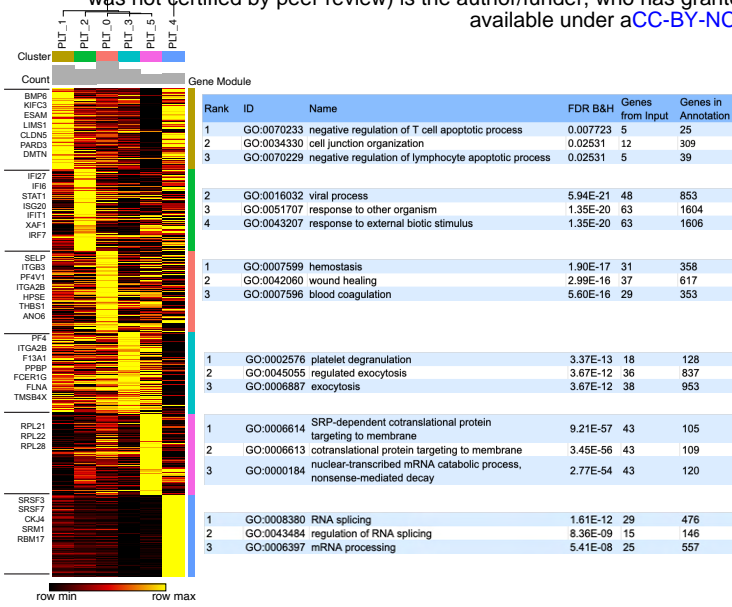


Figure S12. Gene expression signatures of cell types and subtypes activated by COVID-19 are extensively associated with coagulation, hemostasis, and thrombosis-associated pathways, functions, and knockout phenotypes, relative to Figure 4.

A



B

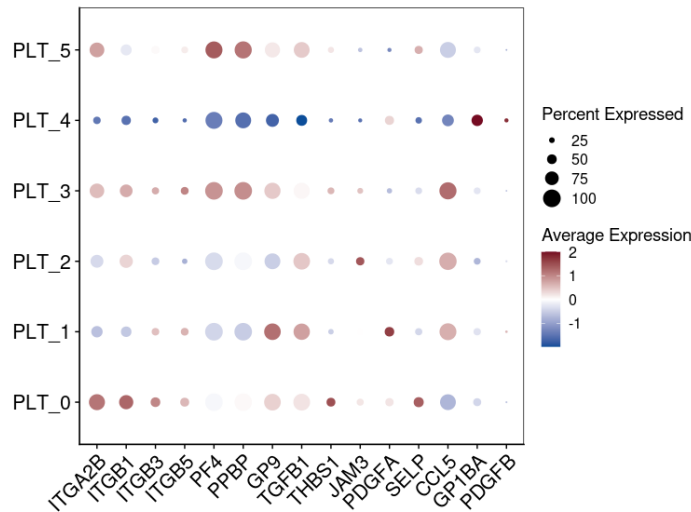


Figure S13. Emergence of platelet subtypes suggestive of functionally significant alternative roles in in hemostasis, coagulation, wound response, and neutrophil recruitment and activation, relative to Figure 4.

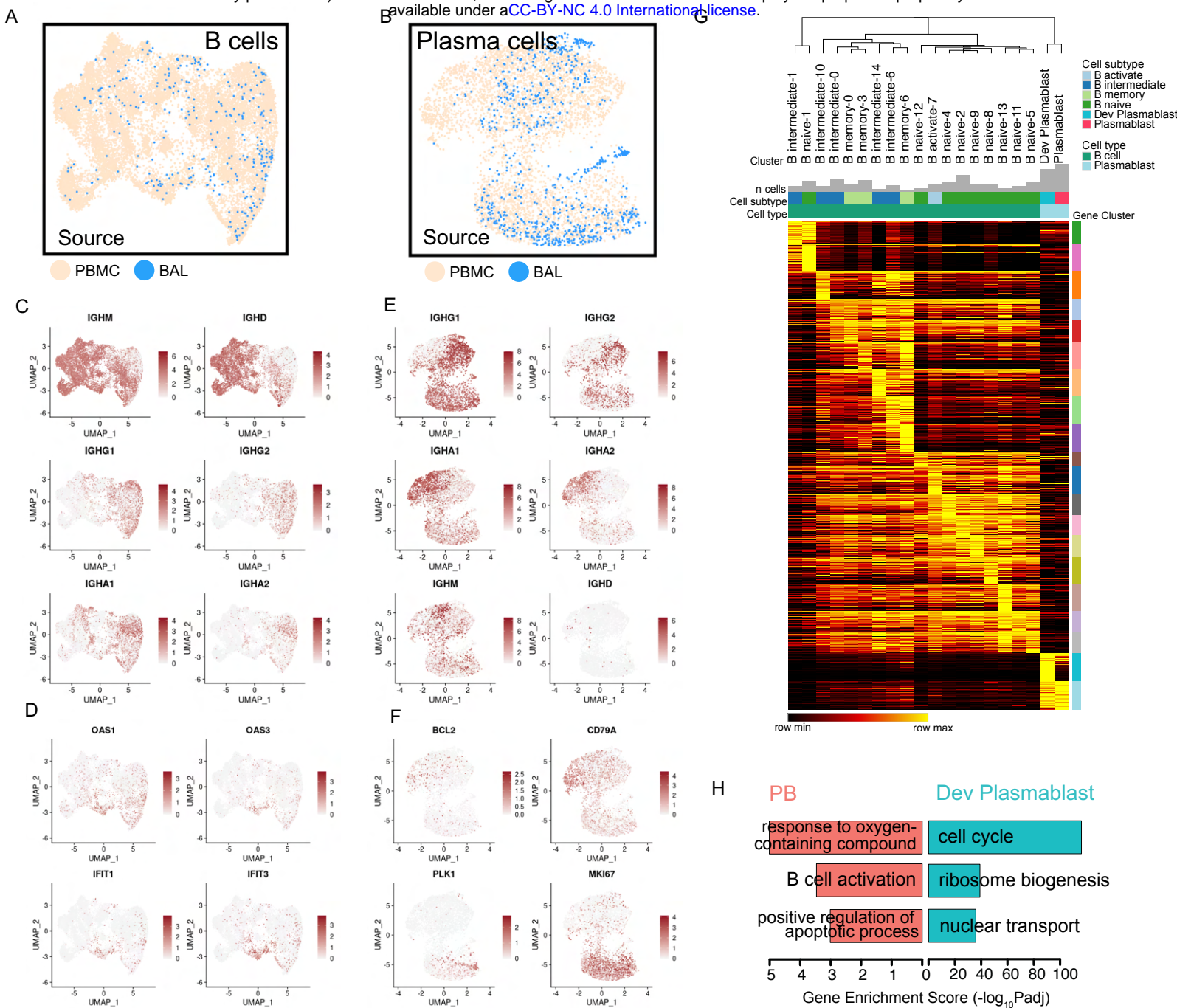


Figure S14. Consistent emergence of a series of early and maturing B cells and plasmablasts in BAL fluid and PBMC across multiple datasets, relative to Figure 5.

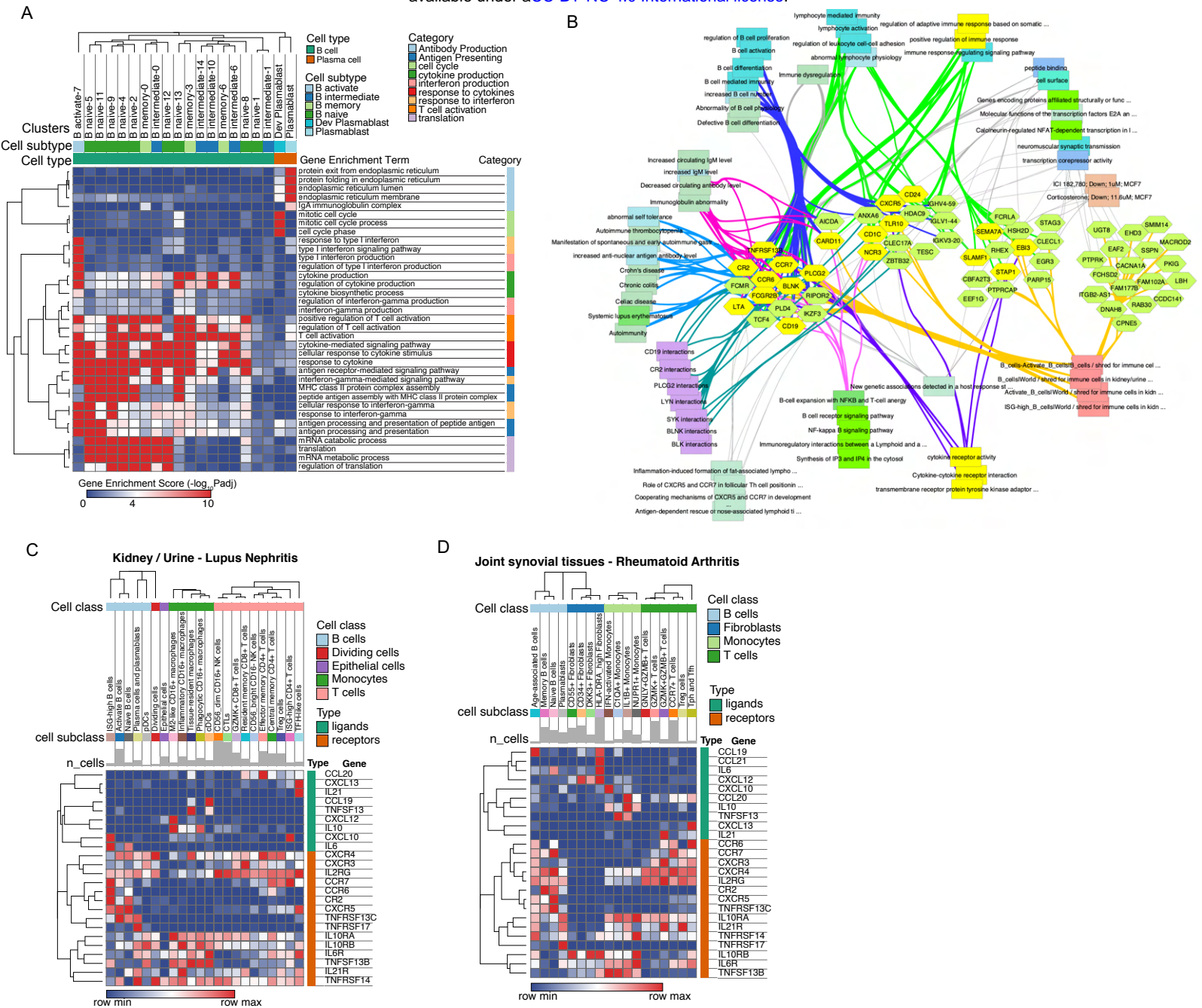


Figure S15. Gene Enrichment analysis of B cell subtypes and autoimmune-associated signatures, relative to Figure 5.

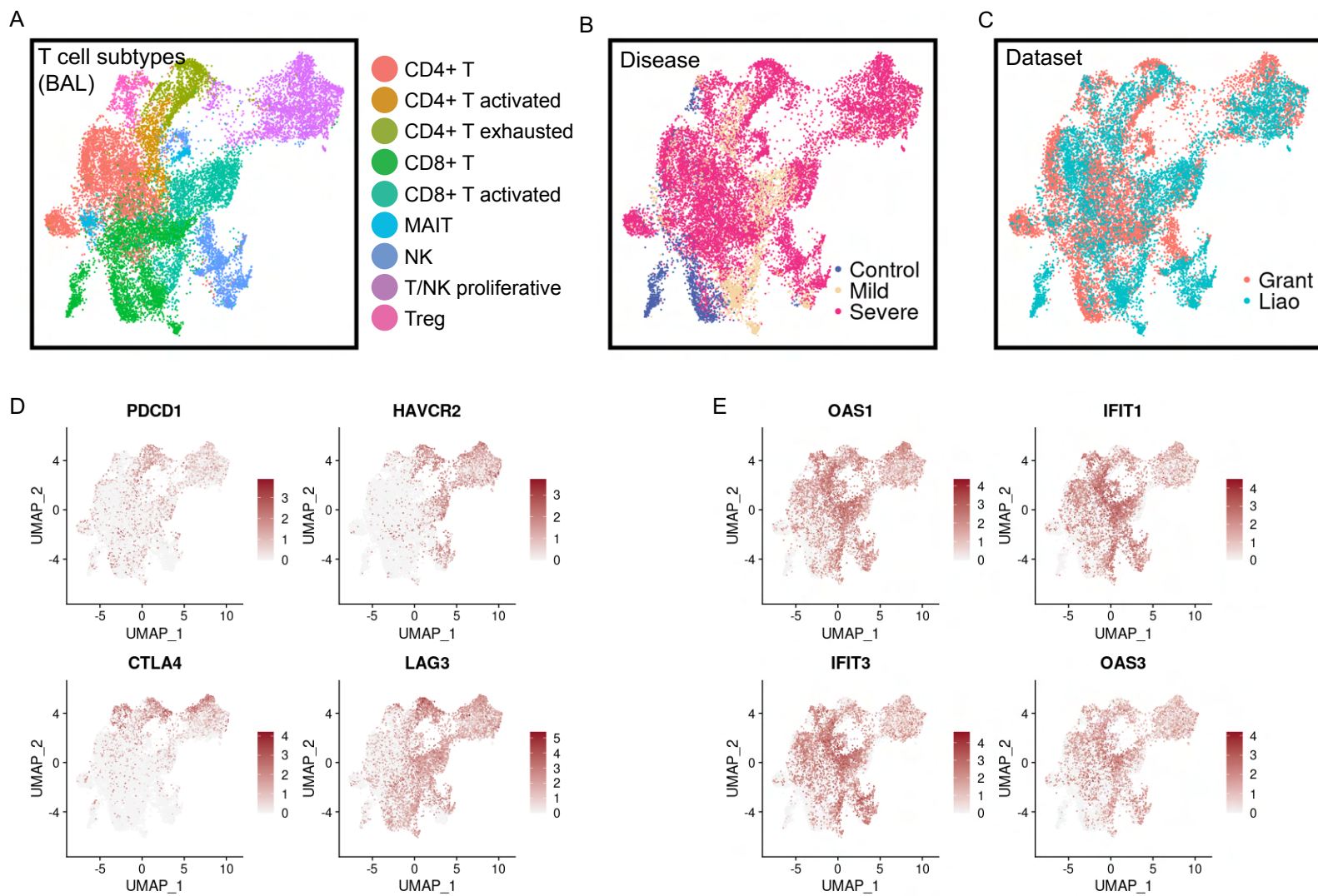
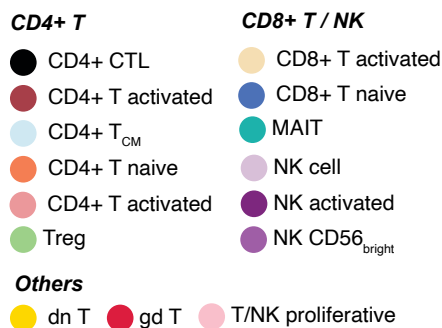
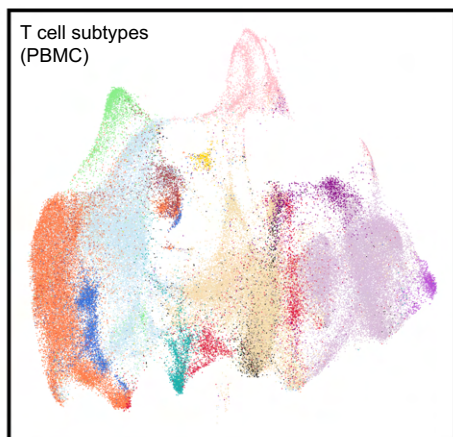
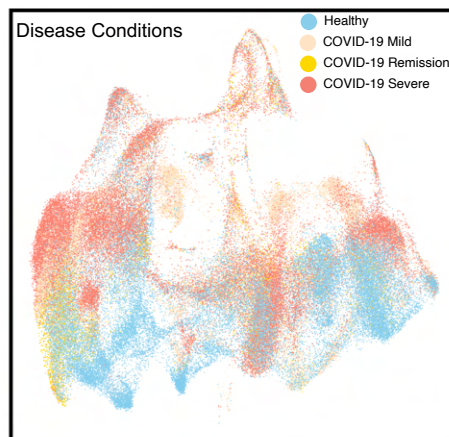


Figure S16. Distinct subtypes of T cells and NK cells in COVID-19 BAL data.

A



B



C

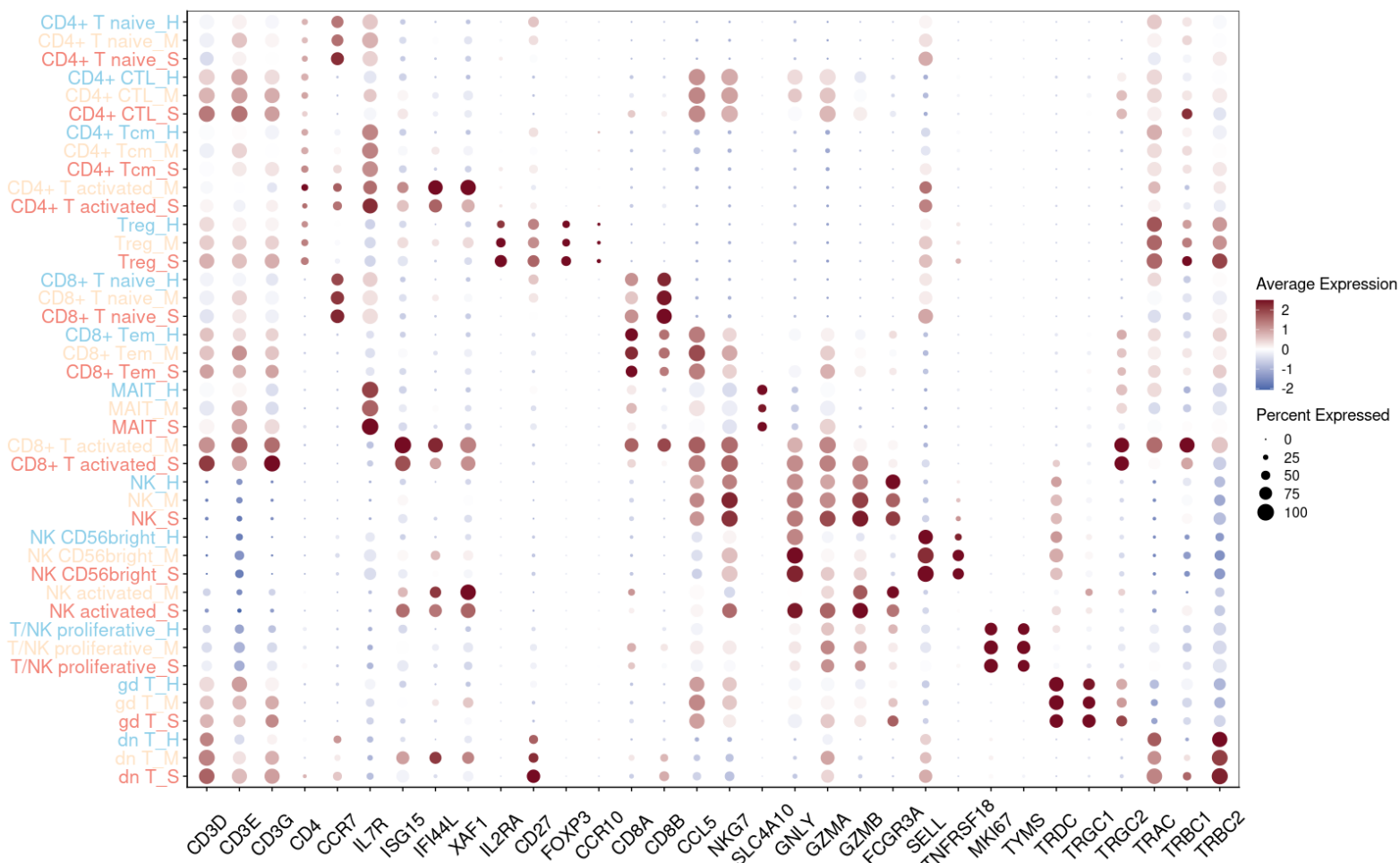
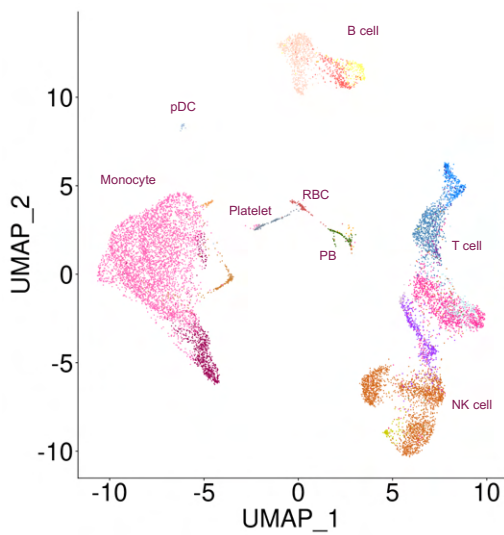


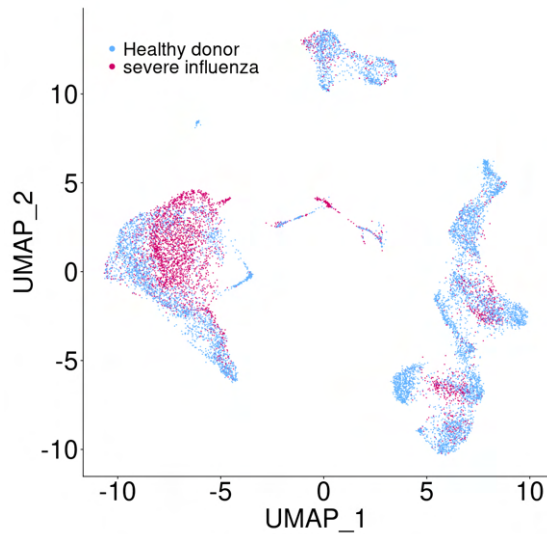
Figure S17. Various T cell and NK cell subtypes in the integrated PBMC data.

A

Influenza

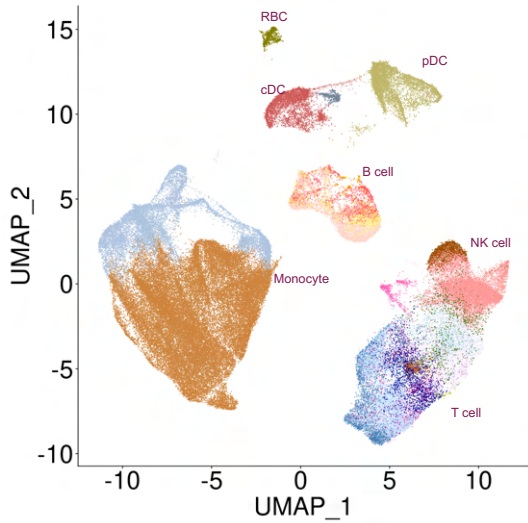


B

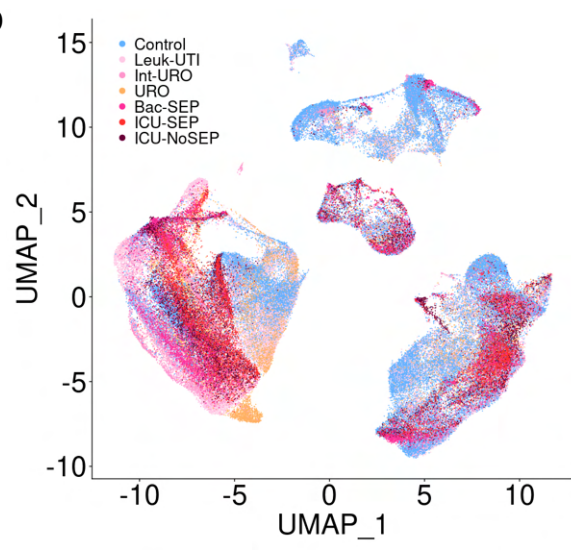


C

Sepsis

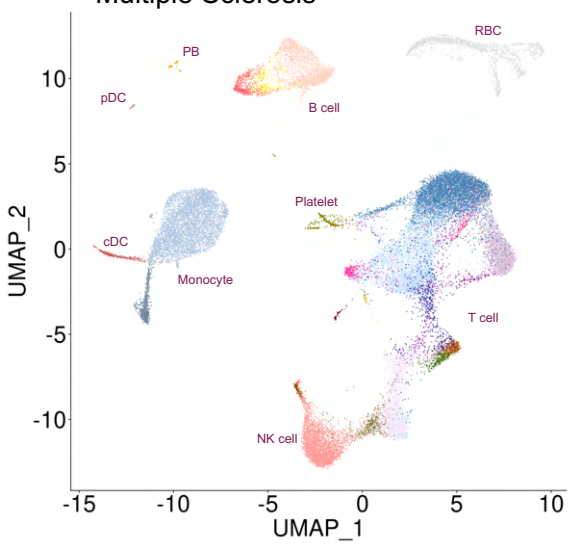


D



E

Multiple Sclerosis



F

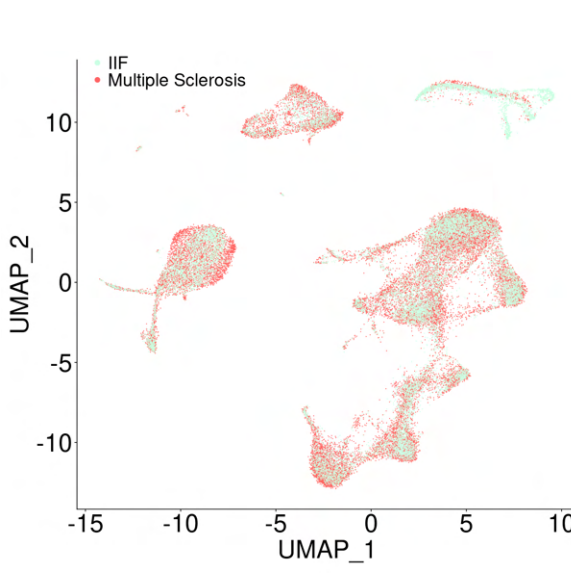


Figure S18. Various cell types in immune-mediated diseases, relative to Figure 7.